Title

Effects of Transverse Steel on the Axial-Compression Strength of FRP-Confined Reinforced Concrete Columns Based on a Numerical Parametric Study

Journal
Journal of Composites for Construction, 25(4)

ISSN
1090-0268

Authors
Zignago, Diogo
Barbato, Michele

Publication Date
2021-08-01

DOI
10.1061/(asce)cc.1943-5614.0001135

Effects of transverse steel on the axial compression strength of FRP-confined reinforced concrete columns based on a numerical parametric study

Diogo Zignago[1]; Michele Barbato[2], M.ASCE
[1]Ph.D. Candidate, Dept. of Civil and Environmental Engineering, Univ. of California Davis, One Shields Ave., Davis, CA 95616. Email: zignago@ucdavis.edu
[2]Professor, Dept. of Civil and Environmental Engineering, Univ. of California Davis, One Shields Ave., Davis, CA 95616 (corresponding author). Email: mbarbato@ucdavis.edu

Abstract

Reinforced concrete (RC) columns can be effectively rehabilitated or strengthened by externally wrapped fiber-reinforced polymer (FRP) wraps, which can improve the axial load capacity and ductility of these columns through a confinement effect. Modern design codes require that seismically designed RC columns have significant minimum amounts of both longitudinal and transverse steel. This transverse steel can apply a considerable confining pressure into the concrete core in addition to that produced by the external FRP sheets. This simultaneous confinement can be accurately modeled using a recently developed FRP-and-steel confined concrete model for finite element analysis. This paper presents a comprehensive parametric study to investigate the steel confinement effects and the relative importance of key modeling and design parameters on the axial strength of FRP-confined RC columns. The results show that the steel confinement effect can significantly increase the axial strength of FRP-confined RC columns, particularly for large cross-sections, low concrete compressive strengths, and low amounts of confining FRP. The steel confinement effects induce two distinct behaviors depending on the ratio between the FRP lateral confinement and the unconfined concrete peak strength. These two behaviors can be described as functions of a relative confinement coefficient. The results of this study could be used to achieve more efficient and economical retrofit of RC columns through FRP confinement.

Keywords: fiber-reinforced polymers; reinforced concrete columns; column retrofit; FRP confinement; steel confinement.

Introduction

Use of fiber-reinforced polymer (FRP) composites for retrofitting reinforced concrete (RC) structures has been extensively investigated throughout the last four decades (Fardis and Khalili 1982; Lam and Teng 2003a; Raza et al. 2019). The utilization of FRP has gained particular attention in recent years as a repair technology to aging RC structures that have their functionality affected by environmental deterioration, damage due to extreme events, or increased demands produced by unplanned loads (Parvin and Brighton 2014). In many cases, the retrofit of RC columns using external FRP jackets or wraps represents a reasonable and cost-effective alternative to steel jackets or enlarged RC cross-sections (Fardis and Khalili 1982; Rocca 2007; Roy et al. 2010). Among the possible applications, FRP wraps can be used to increase the axial compression strength of RC members by producing a confinement effect (Nanni and Bradford 1995; Toutanji 1999; ACI 2017). Whereas RC members that are subject to axial compression only are quite rare in buildings and other structures, axial compression strength of FRP-confined columns has been widely investigated (Spoelstra and Monti 1999; Matthys et al. 2006; Rocca et al. 2006; Hu and Barbato 2014; Piscesa et al. 2018), is explicitly addressed in modern design codes and guidelines (e.g., ACI 2017), and needs to be evaluated when constructing the axial force-bending moment interaction diagram for an RC column (Bank 2006). Axial rehabilitation of RC columns using FRP confinement is also common in practical applications (Parvin and Brighton 2014).

The design of RC columns using modern design standards generally requires a ductile behavior, which leads to relatively higher volumetric ratios of transverse steel reinforcement when compared to columns designed using older standards (Roy et al. 2010). However, the presence of transverse steel reinforcement is generally neglected in the retrofit and rehabilitation of RC columns using FRP wraps, e.g., when using the ACI 440.2R-17 (ACI 2017) guidelines. This situation is probably due to the fact that, whereas the behavior of concrete confined by FRP only is extensively studied and documented in the literature (Fardis and Khalili 1982; Mirmiran and Shahawy 1996; Karbhari and Gao 1997; Samaan et al. 1998; Spoelstra and Monti 1999; Toutanji 1999; Xiao and Wu 2000; Fam and Rizkalla 2001; Lam and Teng 2003a; b; Shao et al. 2006), only a few studies have investigated the simultaneous confining mechanisms of FRP and steel (Demers and Neale 1999; Eid et al. 2009; Wang et al. 2012). Moreover, most of the existing stress-strain models of FRP-and-steel confined concrete use a linear superposition of the confining effects of each material (Li et al. 2003; Ilki et al. 2008; Hu and Seracino 2014), and/or are based on regression analyses of limited data points (Lee et al. 2010), which may lead to inaccurate estimates of the axial strength of FRP-confined RC columns with parameters laying outside the models' calibration ranges. Teng et al. (2015) proposed a model that considers the peak strength of simultaneously confined concrete as a linear superposition of the global contributions from the unconfined concrete strength, FRP, and steel, with the latter being a nonlinear function of the FRP reinforcement ratio.

An FRP-and-steel confined concrete constitutive model based on an incremental procedure that efficiently accounts for the nonlinear interaction of FRP and steel confinement was recently developed to model the stress-strain behavior of confined concrete within the cross-section of FRP-confined circular RC columns (Zignago et al. 2018). This model, used in conjunction with a force-based frame finite element (FE) with fiber-based cross-sections (Hu and Barbato 2014), was thoroughly validated and shown to produce accurate estimates of the structural response of FRP-confined circular RC columns subject to different loading conditions for any realistic combination of design parameters and material properties.

This paper investigates the effects of transverse steel confinement on the axial strength of FRP-confined circular RC columns through an extensive parametric study by using these efficient and accurate nonlinear FE and FRP-and-steel confined concrete models (Hu and Barbato 2014; Zignago et al. 2018). The paper considers wide but realistic ranges of the different design parameters to quantify their relative importance and suggest possible improvements of existing design guidelines. To the authors' knowledge, this is the first study to investigate systematically the issue of simultaneous confinement of RC columns by FRP and steel to understand its effects on the structural behavior of RC members retrofitted using FRP wrapping. This study also identifies easy-to-compute parameters that can synthetically describe the effects of transverse steel on the design strength of the structural members under consideration. The characterization of these parameters represents a preliminary but necessary step towards the improvement of existing design equations for FRP-confined RC columns subject to axial compression.

FE Modeling of FRP-Confined RC Columns

This study estimates the axial strength of FRP-confined columns by using nonlinear FE analysis performed via the general-purpose software framework Open System for Earthquake Engineering Simulation (OpenSees) (Mazzoni et al. 2006). By assuming a concentric axial load condition applied to a short column, the axial strength of the column is calculated as the column sectional capacity using a zero-length fiber-section element (Mazzoni et al. 2006). The material nonlinearity is modeled by associating to the different fibers in the cross-section the appropriate uniaxial stress-strain constitutive models for the corresponding material. Both concrete cover and core fibers within the cross-section are modeled using the FRP-and-steel confined concrete model developed by Zignago et al. (2018), which reduces to the Spoelstra-Monti model (Spoelstra and Monti 1999) for concrete fibers confined by FRP only (i.e., concrete cover confined by FRP), to the Mander model (Mander et al. 1988) for concrete fibers confined by steel only (i.e., core concrete when no FRP is applied), and to the Popovics-Saenz model (Popovics 1973; Balan et al. 1997) for unconfined concrete fibers (i.e., concrete cover when no FRP is applied). A clear concrete cover thickness t_c = 25 mm is assumed for all column models. The unconfined concrete initial tangent modulus, E_c, is calculated as a function of the unconfined concrete compressive peak strength, f_c', as (Mander 1983):

$$E_c = 5000\sqrt{f_c'}\ \text{(MPa)} \tag{1}$$

The unconfined concrete strain at peak strength, ε_c', is calculated using the equation proposed by De Nicolo et al. (1994), which was obtained through regression analysis of experimental results from compressive tests of concrete cylinders collected from several different authors, as:

$$\varepsilon_c' = 0.00076 + \left[\left(0.626 f_c' - 4.33\right)\cdot 10^{-7}\right]^{0.5}\ \text{(MPa)} \tag{2}$$

The maximum allowable strain of the concrete, $\varepsilon_{c,\max}$, is assumed equal to the value specified by ACI 440.2R-17 (ACI 2017) as:

$$\varepsilon_{c,\max} = \varepsilon_c' \cdot \left[1.5 + 12\kappa_b \cdot \frac{f_{lf}}{f_c'} \cdot \left(\frac{\varepsilon_{fe}}{\varepsilon_c'}\right)^{0.45}\right] \leq 0.01 \tag{3}$$

where κ_b is the geometry efficiency factor and is equal to 1 for circular cross-sections; $\varepsilon_{fe} = \kappa_\varepsilon \varepsilon_{fu}$ denotes the effective strain of the FRP at failure, in which κ_ε is the FRP strain efficiency factor determined by using the model proposed by Realfonzo and Napoli (2011) as a function of concrete strength and FRP confining stiffness $K_f = 0.5\rho_f E_f$ (with ρ_f = FRP volumetric reinforcement ratio and E_f = FRP elastic modulus), and ε_{fu} denotes the ultimate strain of the FRP obtained from flat coupon tensile tests; and $f_{lf} = \kappa_\varepsilon f_{lfu}$ is the maximum confinement pressure exerted by the FRP, where f_{lfu} is the ultimate FRP lateral confining pressure. It is observed here that the FRP strain efficiency factor model proposed by Realfonzo and Napoli (2011) decreases linearly for increasing FRP confining stiffness K_f, which also implies that κ_ε increases for increasing column diameter, when everything else is being kept the same. The Menegotto-Pinto plasticity model (Menegotto and Pinto 1973), as modified by Filippou et al. (1983) to include isotropic hardening effects, is used to model the longitudinal steel rebars. The sectional analyses are performed by applying quasi-static, monotonically increasing, and concentric axial loads.

Parametric Study

The parameters considered in this study are: (1) fiber type, i.e., carbon FRP (CFRP) or glass FRP (GFRP); (2) FRP volumetric reinforcement ratio, with six different levels for each type of fiber, i.e., ρ_f = 0%, 0.25%, 0.5%, 1%, 2%, and 3% for CFRP, and ρ_f = 0%, 0.5%, 1%, 2%, 4%, and 6% for GFRP; (3) column diameter, with four different diameters, i.e., D = 150 mm, 300 mm, 600 mm, and 1,200 mm; (4) concrete compressive strength, with four different strength levels, i.e., f_c' = 20 MPa, 30 MPa, 50 MPa, and 70 MPa; and (5) transverse steel volumetric reinforcement ratio, with six different levels, i.e., ρ_{st} = 0%, 0.5%, 1%, 2%, 3%, and 4%. The combination of the different values for all the parameters results in a total of 1,152 nonlinear FE analyses. Table 1 summarizes the parameters considered and their values, whereas Table 2 shows the material properties considered as constants and their values used in the FE simulations.

The ultimate tensile strength, f_{fu}, and modulus of elasticity, E_f, of the CFRP material are two and four times larger than those of the GFRP material, respectively, leading to an ultimate strain for the GFRP sheets twice as large as that for the CFRP sheets. The GFRP reinforcement ratios are selected to be twice those for CFRP to allow for an easier comparison of both FRP ultimate lateral confining pressure, f_{lfu}, and FRP confining stiffness, K_f, for the different fiber types. The range of the transverse steel reinforcement ratio, ρ_{st}, is selected to be between 0%, i.e., no stirrups or ties, and 4%, which represents a practical upper limit for real-world applications, as it is a slightly higher value than that obtained from the shear strength caps given in Provision 11.4.3 of ACI 440.2R-17 (ACI 2017).

Parametric Study Results

The parametric study results are expressed here in terms of the peak axial strength, $\bar{P}_{\max}$ or $P_{\max}$, for the different columns. Hereinafter, quantities with a superposed bar represent strengths obtained by imposing the design limitation on concrete deformation given by Eq. (3); whereas the same symbol without the superposed bar indicates strengths obtained without imposing any limitation on the concrete deformation. In particular, the quantity $\overline{P}_{\max}$ is relevant when making design considerations, for which imposing a limitation on concrete crushing is a desirable feature; whereas the quantity $P_{\max}$ can better describe experimental testing results when specimens are loaded up to their complete failure. In order to separate the confinement effects due to steel only from the FRP confinement effects, two reference axial strengths are considered for each given column: (1) the peak axial strength of the reference unconfined column, P_0 (i.e., a column with the same properties as the given column but with $\rho_f = 0\%$ and $\rho_{st} = 0\%$); and (2) the peak axial strength of the reference FRP-only-confined column without transverse steel, $\overline{P}_{f0}$ and P_{f0} (i.e., i.e., a column with the same properties as the given column but with $\rho_{st} = 0\%$). It is noteworthy that, for the reference unconfined column, the peak axial strengths obtained by imposing or not imposing the concrete deformation limit given by Eq. (3) coincide (i.e., $P_0 = \overline{P}_0$), as the columns reach their peak axial strengths at a concrete strain $\varepsilon_c = \varepsilon_c' < \varepsilon_{c,\max}$. For easy comparison, all strength results are presented hereinafter in non-dimensional form, as relative strength increments normalized by P_0.

Increment in peak axial strength due to simultaneous steel and FRP confinement

Figure 1(a) through (d) summarize the effects of FRP confining stiffness, column diameter, concrete compressive strength, and transverse steel ratio, respectively, on the peak axial strength's normalized total increment $\left(\overline{P}_{\max} - P_0\right)/P_0$. The results are presented in the form of box-and-whisker plots (Cleveland 1985) and exclude the data points for which $\rho_f = 0\%$ or $\rho_{st} = 0\%$. The central horizontal line of each plot represents the median value, with the bottom and top edges of the boxed area indicating the first and third quartile of the data, respectively. The whiskers identify the complete range of the data. The notches in the boxed area display the confidence interval around the median.

Figure 1(a) shows that $\left(\bar{P}_{\max}-P_0\right)/P_0$ significantly increases for increasing FRP confining stiffness, even though not monotonically. The median value of $\left(\bar{P}_{\max}-P_0\right)/P_0$ increases from approximately 29% for K_f = 62.5 MPa to approximately 97% for K_f = 1.5 GPa. More dispersion in the results is found for low FRP reinforcement ratios. This result was expected, as the beneficial effect of FRP-confinement on the concrete compressive strength is well-known (Fardis and Khalili 1982; Karbhari and Gao 1997). Figure 2 plots $\left(\bar{P}_{\max}-P_0\right)/P_0$ as a function of the ratio between the FRP confining pressure and the unconfined concrete strength, $f_{lf}\ /\ f'_c$ (referred to as FRP confinement ratio hereinafter), which is known to be strongly positively correlated with the FRP-confined concrete peak strength, f'_{cc} (Fardis and Khalili 1982; Spoelstra and Monti 1999; Lam and Teng 2003a).

Figure 2 also reports the trendline of the numerical simulation results in conjunction with its coefficient of determination, R^2 = 0.699. This trendline is computed based on a quadratic/linear rational function (i.e., a rational function in which numerator and denominator are polynomials of order 2 and 1, respectively). The vertical dashed line represents the value $f_{lf}\ /\ f'_c = 0.08$, which is the lower limit for FRP confinement recommended in ACI 440.2R-17 (ACI 2017). The relatively low value of the coefficient of determination indicates a large dispersion of the data points. Based on the trendline, it is observed that, for the lower values of the FRP confinement ratio (i.e., $f_{lf}\ /\ f'_c < 0.05$), $\left(\bar{P}_{\max}-P_0\right)/P_0$ increases almost proportionally with $f_{lf}\ /\ f'_c$, whereas for the higher values of the FRP confinement ratio (i.e., $f_{lf}\ /\ f'_c > 0.10$), the increase of $\left(\bar{P}_{\max}-P_0\right)/P_0$ rapidly slows down, until only small increases are observed when $f_{lf}\ /\ f'_c > 0.30$. It is concluded that, for small amounts of FRP, $\overline{P}_{\max}$ is mainly controlled by the FRP confinement ratio; whereas, for large amounts of FRP (and in particular for $f_{lf} / f_c' \geq 0.08$), $\overline{P}_{\max}$ is mainly controlled by the FRP confining stiffness. It is also observed that the value of the trendline for $f_{lf} / f_c' = 0$ (i.e., no FRP confinement) is approximately equal to 12%, which provides an approximate measure of the average effect of the transverse steel confinement on the core concrete for the range of geometries and material parameters considered in this study.

Figure 1(b) shows that $\left(\overline{P}_{\max} - P_0\right)/P_0$ slightly increases as the column diameter increases. This effect is less significant than that of the FRP confining stiffness, but it is not negligible. In fact, the median value of $\left(\overline{P}_{\max} - P_0\right)/P_0$ increases from approximately 45% when $D = 150$ mm to approximately 66% for columns with $D = 1200$ mm. By contrast, the interquartile range is found to be almost independent of the diameter. The observed influence of the diameter on $\left(\overline{P}_{\max} - P_0\right)/P_0$ is attributed to the increase in the cross-sectional core to gross area ratio, A_c / A_g, for increasing column diameter, which is produced by the modeling choice of keeping the concrete cover's thickness as constant and equal to 25 mm for all column diameters. Because the concrete core is subjected to the combined confinement of both FRP and steel, whereas the concrete cover is subjected to the confinement of the FRP only, an increase of A_c / A_g is likely to produce an increase in the peak axial strength. To test this hypothesis, four additional numerical simulations were performed by setting $A_c / A_g = 0.840$ (i.e., the ratio corresponding to a column with $D = 600$ mm and $t_c = 25$ mm), considering the same four column diameters used in the parametric study (i.e., $D = 150$ mm with $t_c = 6.25$ mm, $D = 300$ mm with $t_c = 12.5$ mm, $D = 600$ mm with $t_c = 25$ mm, and $D = 1200$ mm with $t_c = 50$ mm), and assuming the following constant values for the other variables: concrete strength $f_c' = 30$ MPa, CFRP reinforcement ratio $\rho_f = 1\%$, and steel reinforcement ratio $\rho_{st} = 4\%$. The steel confinement effectiveness coefficient was also kept constant and equal to $k_s = 0.99$ (Mander et al. 1988). The four additional FE analyses produced the same value of $(\bar{P}_{\max} - P_0) / P_0 = 106.8\%$, which confirms that the gain in strength observed in Figure 1(b) is due to the increase of A_c / A_g.

Figure 1(c) shows that $\left(\bar{P}_{\max} - P_0\right)/P_0$ drastically decreases for increasing values of f_c'. This result is consistent with existing confined concrete models that describe the relative gain in strength of confined concrete, i.e., $(f_{cc}' - f_c') / f_c'$, as inversely proportional (Richart et al. 1929; Lam and Teng 2003a) or approximately inversely proportional (Mander et al. 1988) to the unconfined concrete strength f_c'. Figure 1(c) also shows a larger scatter of the results for lower strength concretes, which present a larger interquartile range than higher strength concretes.

Figure 1(d) shows an approximately linear increase in the median of $\left(\bar{P}_{\max} - P_0\right)/P_0$ for increasing values of ρ_{st}. The interquartile range of these results is almost independent of the reinforcement level. This result was also expected, as the additional confinement effect due to the transverse steel generally increases the confined concrete's peak strength, f_{cc}' (Zignago et al. 2018).

The results presented in Figure 1, albeit expected, lead to the conclusion that both the transverse steel volumetric ratio, ρ_{st}, and the column diameter, *D*, have significant beneficial effects on the peak axial strength of FRP-confined columns. This conclusion is important because current design codes and guidelines generally neglect the effects of these two parameters on the prediction of the load-carrying capacity of FRP-confined RC columns (ACI 2017).

In order to investigate more in detail the effects of transverse steel confinement on the peak axial strength of FRP-confined columns, as well as the interaction among different parameters, Figure 3(a) plots $\left(\bar{P}_{\max} - P_0\right)/P_0$ versus ρ_{st} for columns strengthened with CFRP wraps and with

$f_c' = 30$ MPa, when the amount of FRP and the column diameter are varied. The observed interaction among the different parameters is quite complex. FRP confinement contributes significantly to $\left(\bar{P}_{\max} - P_0\right)/P_0$, e.g., with a value of 91.7% for a CFRP ratio of $\rho_f = 3.0\%$ when $\rho_{st} = 0$, which increases to 134.4% when $\rho_{st} = 4\%$ and $D = 1200$ mm. This increment is independent of the column diameter when no transverse steel is present. The value of $\left(\bar{P}_{\max} - P_0\right)/P_0$ increases rapidly for lower values of ρ_f, up to $\rho_f = 1\%$, whereas it increases in a decreasing fashion for higher values of ρ_f, indicating a diminishing effectiveness of the FRP confinement. These results also confirm that steel confinement effect can be significant and that the increase in axial strength of the FRP-confined columns strongly depends on both the column diameter, D, and the transverse steel reinforcement ratio, ρ_{st}. The increase in axial strength due to the steel confinement effect becomes more pronounced going from $\rho_f = 0\%$ with $\max\left[\left(\bar{P}_{\max} - P_0\right)/P_0\right]$ = 34.4%, to $\rho_f = 1.0\%$ with $\max\left[\left(\bar{P}_{\max} - P_0\right)/P_0\right]$ = 68.3%, and then gradually decreases from $\rho_f = 1.0\%$ to $\rho_f = 3.0\%$ with $\max\left[\left(\bar{P}_{\max} - P_0\right)/P_0\right]$ = 44.4%. This result confirms the strong nonlinearity of the combination of FRP and steel confinement effects. It is noted here that similar behaviors were observed also for the other combinations of concrete strength and FRP materials considered in this study.

Figure 3(b) plots $\left(\bar{P}_{\max} - P_0\right)/P_0$ versus ρ_{st} for columns with diameter $D = 600$ mm and confining stiffness $K_f = 0.5$ GPa (which corresponds to $\rho_f = 1\%$ for CFRP or $\rho_f = 4\%$ for GFRP), when the FRP material and the concrete compressive strength are varied. The quantity $\left(\bar{P}_{\max} - P_0\right)/P_0$ always increases for increasing transverse steel ratio, and this increase is more pronounced as the concrete compressive strength decreases. In general, for a fixed value of FRP confining stiffness, $\left(\bar{P}_{\max} - P_0\right)/P_0$ for a column strengthened with GFRP wraps is greater than or equal to that of a column with CFRP sheets. This difference is larger for higher concrete compressive strengths and it gradually decreases with f'_c, until no differences are observed between columns strengthened with GFRP and CFRP for f'_c = 20 MPa.

These results can be explained by considering the combination of two phenomena affecting the peak axial strength, $\bar{P}_{\max}$: (1) the limitation on the maximum concrete strain imposed by Eq. (3), which depends on f_{lf} / f'_c until $\varepsilon_{c,\max}$ reaches the value 0.01; and (2) the effects of the FRP and steel confinement, which depend on K_f / E_c and f_{ls} / f'_c, respectively. To investigate more in depth these two phenomena, the FRP-and-steel confined concrete axial stress-strain behavior obtained using the model developed by Zignago et al. (2018) is plotted in Figure 4 for a concrete with f'_c = 30 MPa with four levels of FRP confining stiffness to concrete elastic modulus ratio (i.e., K_f / E_c = 0.0023, 0.0046, 0.0092, and 0.0274), and four levels of steel confinement ratio (i.e., f_{ls} / f'_c = 0, 0.05, 0.15, 0.25), for a total of 16 different FRP and transverse steel confinement configurations. These K_f / E_c levels correspond to GFRP reinforcement ratios ρ_f = 0.5%, 1%, 2%, and 6%, respectively, and to CFRP reinforcement ratios ρ_f = 0.125%, 0.25%, 0.5%, and 1.5%, respectively; whereas the considered f_{ls} / f'_c levels correspond to transverse steel ratios $\rho_{st} = 0\%$ (identified by thicker lines), 0.67%, 2.0%, and 3.33%, respectively, and a constant steel confinement effectiveness coefficient $k_s = 1.00$ (Mander et al. 1988). Figure 4 also provides: the axial strains at which the GFRP and CFRP wraps fail, $\varepsilon_{c,fu}$ (identified by filled markers); the maximum allowable concrete compressive strain based on Eq. (3), $\varepsilon_{c,\max}$, for each fiber type (identified by unfilled markers); and the axial strains at which the transverse steel yields, $\varepsilon_{c,sy}$ (identified by crosses). It is important to note that, for given properties of the unconfined concrete and confining steel, the confined concrete axial stress-axial strain curve is fully determined by the values of K_f / E_c and f_{ls} / f_c', and that the only difference among various fiber materials is the axial strain at which the fibers fail, which is determined by their effective strain at failure, ε_{fe}.

The FRP-confined concrete stress-strain curves in Figure 4 can be classified into three categories (Lam and Teng 2003a): type I curves, which correspond to low confinement levels and have post-peak decreasing branches with a concrete ultimate stress $f_{cu} < f_c'$, e.g., the thick curve reported in Figure 4(a); type II curves, which correspond to moderate confinement levels and have post-peak branches with a softening or flat portion followed by a hardening portion with $f_{cu} > f_c'$, e.g., the thick curve reported in Figure 4(b); and type III curves, which correspond to high confinement levels and are monotonically increasing everywhere, e.g., the thick curves reported in Figure 4(c) and (d). The stress-strain behavior of concrete confined simultaneously by steel and FRP generally have the same characteristics of the stress-strain behavior of FRP-confined concrete. Therefore, it is concluded that the compressive strain at which an FRP-confined RC column reaches its peak strength corresponds to the maximum allowable compressive strain of the concrete, $\varepsilon_{c,\max}$, when the confinement effect is sufficient to achieve a type III curve; whereas it is contained between ε_c' and $\varepsilon_{c,\max}$ when the confinement effect is limited and the concrete stress-strain behavior correspond to a type I or type II curve.

From Figure 4, it is also observed that, as K_f / E_c increases, the $\varepsilon_{c,\max}$ increases faster for GFRP than for CFRP, until the $\varepsilon_{c,\max}$ for GFRP reaches the upper limit of 0.01, at which point only the $\varepsilon_{c,\max}$ for the CFRP keeps increasing until it also reaches the value of 0.01. This phenomenon contributes to the faster increase followed by a slower increase of $\left(\bar{P}_{\max} - P_0\right) / P_0$ for increasing ρ_f, which is observed in Figure 3(a). It also explains why, for a given f_c' and any level of ρ_{st}, the value of $\left(\bar{P}_{\max} - P_0\right) / P_0$ for GFRP confinement is higher than or equal to that for CFRP confinement, as observed in Figure 3(b). In particular, the equal peak axial strength of RC columns confined with GFRP and CFRP for f_c' = 20 MPa is due to the fact that, for the given level of FRP confining stiffness, the value of $\varepsilon_{c,\max}$ has already reached the upper limit of 0.01 for both fiber types, similar to the case shown in Figure 4(d). The differences in $\left(\bar{P}_{\max} - P_0\right)/P_0$ for the two types of fiber at any given value of K_f is amplified for increasing values of f_c' because the FRP-confining stiffness ratio, K_f/E_c, decreases due to the proportionality between E_c and $\sqrt{f_c'}$ given by Eq. (1).

Figure 4 also shows that, for low levels of K_f/E_c (i.e., low values of $\varepsilon_{c,\max}$) and (in minor measure) of f_{ls}/f_c' (i.e., high values of $\varepsilon_{c,sy}$), yielding of the transverse steel can take place at strains larger than $\varepsilon_{c,\max}$ (i.e., $\varepsilon_{c,sy} > \varepsilon_{c,\max}$), thus preventing the transverse steel confining mechanism from being fully utilized. By contrast, when $\varepsilon_{c,sy} < \varepsilon_{c,\max}$, the transverse steel confining mechanism can fully develop. This phenomenon is the major contributor to the rapid increase in $\left(\bar{P}_{\max} - P_0\right)/P_0$ observed in Figure 3(a) for low values of ρ_f going from 0% to 1.0%, as the corresponding increase in K_f/E_c gradually allows full development of the transverse steel confining mechanism.

Effects of concrete strain design limit on column peak axial strength

Figure 5 shows the relative peak axial strength increment $\left(P_{\max} - \bar{P}_{\max}\right)/P_0$ obtained by removing the design limitation on concrete axial strain given by Eq. (3). In particular, Figure 5(a) plots $\left(P_{\max} - \bar{P}_{\max}\right)/P_0$ versus ρ_{st} for columns strengthened with CFRP wraps and with f_c' = 30 MPa, when the amount of FRP and the column diameter are varied; whereas Figure 5(b) plots $\left(P_{\max} - \bar{P}_{\max}\right)/P_0$ versus ρ_{st} for columns with diameter $D = 600$ mm and confining stiffness K_f = 0.5 GPa, when the FRP material and the concrete compressive strength are varied.

The results in Figure 5(a) show that the columns most impacted by the concrete strain limitation are those with low amounts or no FRP, large amounts of transverse steel, and large diameters. As the transverse steel ratio increases, the concrete core's peak strength increases; however, $\varepsilon_{c,\max}$ is not affected by ρ_{st}, and the peak strength for steel-confined concrete and for concrete confined with large amounts of steel and small amounts of FRP is achieved only at axial strains that are often significantly larger than $\varepsilon_{c,\max}$. The quantity $\left(P_{\max}-\overline{P}_{\max}\right)/P_0$ can reach values as high as approximately 66% for columns with $D = 1200$ mm and $\rho_{st} = 4.0\%$ when no limitation is considered. It is observed that, for $\rho_f = 0\%$ and 0.25%, the column diameter has a major effect on $\left(P_{\max}-\overline{P}_{\max}\right)/P_0$, with larger diameters corresponding to large values of $\left(P_{\max}-\overline{P}_{\max}\right)/P_0$ and smaller diameters corresponding to small values of $\left(P_{\max}-\overline{P}_{\max}\right)/P_0$ (almost negligible for $D = 150$ mm). This phenomenon results from two effects: (1) the steel confinement effectiveness, k_s, decreases rapidly for decreasing column diameters and constant ρ_{st}; (2) the transverse steel confinement effect increases for increasing column diameters, as the ratio A_c / A_g also increases. $\left(P_{\max}-\overline{P}_{\max}\right)/P_0$ increases for increasing values of ρ_{st} and D for all columns with $\rho_f = 0.0\%$ and 0.25%, and for columns with $\rho_f = 0.5\%$ and $\rho_{st} \geq 2\%$. These cases correspond to columns in which the transverse steel reaches yielding at strains larger than $\varepsilon_{c,\max}$, as shown in Figure 4(a) through (c). For $\rho_f = 0.5\%$, there is a change of behavior between the cases with $\rho_{st} < 2\%$ and $\rho_{st} \geq 2\%$: $\left(P_{\max}-\overline{P}_{\max}\right)/P_0$ decreases for ρ_{st} increasing from 0% to 1.0% and increasing column diameter, before increasing again for $\rho_{st} \geq 2\%$. For larger amounts of CFRP (i.e., $\rho_f \geq 1.0\%$), $\left(P_{\max}-\overline{P}_{\max}\right)/P_0$ always slightly decreases for increasing ρ_{st} and D. This phenomenon is the result of two contrasting effects: (1) $P_{\max}$ increases more than $\overline{P}_{\max}$ for increasing values of ρ_f as the confined concrete stress-strain curve moves from a type I or type II curve to a type III curve, and the axial strain corresponding to FRP failure, $\varepsilon_{c,fu}$, is significantly larger than $\varepsilon_{c,\max}$ (see Figure 4); and (2) as ρ_f increases, a larger portion of the transverse steel contribution to the peak axial strength takes place before the axial strain reaches $\varepsilon_{c,\max}$ (i.e., the transverse steel contribution to $\bar{P}_{\max}$ increases more than its contribution to $P_{\max}$).

The results in Figure 5(b) show that, for any value of f_c' and ρ_{st}, $\left(P_{\max}-\bar{P}_{\max}\right)/P_0$ is always higher for GFRP-confined columns than for CFRP-confined columns. This results is due to two superposing effects: (1) for a given K_f/E_c, $P_{\max}$ is higher for RC columns confined with GFRP than for those confined with CFRP because of the higher values of ε_{fe} and, thus, of $\varepsilon_{c,fu}$ for GFRP than for CFRP; and (2) the GFRP-confined concrete reaches the upper limit $\varepsilon_{c,\max}=0.01$ at a lower value of f_{lf}/f_c' than CFRP-confined concrete, thus reaching a cap for $\bar{P}_{\max}$ at lower values of K_f/E_c. For example, assuming the average value $\kappa_\varepsilon = 0.65$ suggested by Realfonzo and Napoli (2011), $\varepsilon_{c,\max}=0.01$ is reached at $f_{lf}/f_c' = 0.158$ for CFRP and at $f_{lf}/f_c' = 0.116$ for GFRP. It is also observed that, for GFRP, $\left(P_{\max}-\bar{P}_{\max}\right)/P_0$ decreases for increasing f_c' and ρ_{st}, with values as high as approximately 60% for $f_c' = 20$ MPa and $\rho_{st} = 0\%$, and as low as 17% for $f_c' = 70$ MPa and $\rho_{st}=4\%$; whereas for CFRP, the value of $\left(P_{\max}-\bar{P}_{\max}\right)/P_0$ presents only a small variability between 8% and 19% for all considered values of f_c' and ρ_{st}, without a monotonic trend with respect of these two variables.

Effects of transverse steel confinement on peak axial strength of FRP-confined columns

Figure 6(a) through (d) summarize the effects of FRP confining stiffness, column diameter, concrete compressive strength, and transverse steel ratio, respectively, on $\left(\bar{P}_{\max}-\bar{P}_{f0}\right)/P_0$. These results separate the transverse steel confinement effects on the peak axial strength of FRP-confined RC columns from the global effects due to the simultaneous FRP and steel confinement. Similar to Figure 1, these results are presented in the form of box-and-whisker plots (Cleveland 1985) and exclude the data points for which $\rho_f = 0\%$ or $\rho_{st} = 0\%$.

Figure 6(a) shows that $\left(\bar{P}_{\max} - \bar{P}_{f0}\right)/P_0$ decreases significantly for increasing values of K_f, with the median value going from approximately 27% for K_f = 62.5 MPa to approximately 13% for K_f = 1.5 GPa. This trend is the opposite of that observed in Figure 1(a) and indicates that the transverse steel confinement effects become less important for increasing amounts of FRP confinement, confirming the strongly nonlinear global behavior associated with the interaction between the FRP and steel confining mechanisms. The variability of the results, as indicated by both the interquartile ranges and the entire data ranges, is drastically reduced as K_f increases.

Figure 7 plots $\left(\bar{P}_{\max} - \bar{P}_{f0}\right)/P_0$ versus f_{lf} / f_c'. It also provides the trendline (based on a quadratic/linear rational function) of the numerical simulation results, which has a coefficient of determination $R^2 = 0.031$, and indicates the value $f_{lf} / f_c' = 0.08$ with a vertical dashed line. This trendline suggests that $\left(\bar{P}_{\max} - \bar{P}_{f0}\right)/P_0$ increases with f_{lf} / f_c' for low values of the FRP confinement ratio (i.e., $f_{lf} / f_c' < 0.05$), whereas it slightly decreases with f_{lf} / f_c' for high values of the FRP confinement ratio (i.e., $f_{lf} / f_c' > 0.10$). These results seem to confirm that the behavior of FRP-confined RC columns changes for FRP confinement ratios that are lower or higher than the lower bound $f_{lf} / f_c' = 0.08$ recommended in ACI 440.2R-17 (ACI 2017). However, the very low value of the coefficient of determination for this trendline indicates that the dispersion of the results is very high and that the dependence of $(\bar{P}_{\max} - \bar{P}_{f0}) / \bar{P}_{f0}$ on f_{lf} / f_c' is most likely not meaningful.

The results in Figure 6(b) show that $\left(\overline{P}_{\max}-\overline{P}_{f0}\right)/P_0$ increases for increasing column diameters, with the median values going from 10.6% for D = 150 mm to 32.2% for D = 1200 mm. This positive correlation is stronger than that observed in Figure 1(b) between $\left(\overline{P}_{\max}-P_0\right)/P_0$ and D. In fact, the increases in the median values of $\left(\overline{P}_{\max}-\overline{P}_{f0}\right)/P_0$ and $\left(\overline{P}_{\max}-P_0\right)/P_0$ from D = 150 mm to D = 1200 mm are both equal to approximately 21%, indicating that this increase is due exclusively to the steel confinement effect. This result is also confirmed by the four additional numerical simulations performed by setting $A_c / A_g = 0.840$, which yield the same value $\left(\overline{P}_{\max}-\overline{P}_{f0}\right)/P_0 = 60.7\%$,

Figure 6(c) shows that both the median and the interquartile range of $\left(\overline{P}_{\max}-\overline{P}_{f0}\right)/P_0$ slightly decreases as f_c' goes from 20 MPa to 70 MPa. As expected, Figure 6(d) shows a drastic increase of both the median and the interquartile range of $\left(\overline{P}_{\max}-\overline{P}_{f0}\right)/P_0$ for increasing values of ρ_{st}. Again, these results are consistent with the steel confinement mechanism and its effects on the axial stress-axial strain behavior observed in Figure 4.

Selection of synthetic parameters to describe the transverse steel confinement effects

The results of the parametric study presented in this paper suggest that the transverse steel confinement effects on the peak axial strength of an FRP-confined RC columns depend on: (1) the ratio of the confinement separately exerted by the steel and the FRP, and (2) the ratio between the core area (confined by both steel and FRP) and the gross area of the columns. Therefore, the following two relative confinement effect coefficients are proposed to synthetically describe the effects of transverse steel confinement on the columns' peak axial strength:

$$c_f = \frac{f_{ls} \cdot A_c}{f_{lf} \cdot A_g} \tag{4}$$

$$C_s = \frac{100 f_{ls} \cdot A_c}{K_f \cdot A_g} \tag{5}$$

It is noteworthy that c_f was originally introduced in Zignago et al. (2018) and used in Zignago and Barbato (2019), where only $P_{\max}$ values were considered; whereas C_s is proposed here for the first time. These two nondimensional coefficients differ in the way they account for the magnitude of FRP confinement. In particular, c_f is a function of the maximum FRP confining pressure f_{lf}, which depends on the effective strain of the FRP at failure, ε_{fe}. Thus, the use of c_f is more appropriate for applications in which failure of the confining FRP is expected, e.g., in the prediction of the ultimate strength of experimental specimens loaded to failure. By contrast, C_s is a function of the FRP confining stiffness K_f, and its use is more appropriate for applications in which failure of the confining FRP should be avoided, e.g., in developing design equations.

Figure 8(a) plots $\left(\overline{P}_{\max} - \overline{P}_{f0}\right) / \overline{P}_{f0}$ versus c_f for $f_{lf} / f_c' \geq 0.08$; Figure 8(b) plots $\left(\overline{P}_{\max} - \overline{P}_{f0}\right) / \overline{P}_{f0}$ versus c_f for $f_{lf} / f_c' < 0.08$; Figure 8(c) plots $\left(P_{\max} - P_{f0}\right) / P_{f0}$ versus c_f for $f_{lf} / f_c' \geq 0.08$; and Figure 8(d) plots $\left(P_{\max} - P_{f0}\right) / P_{f0}$ versus c_f for $f_{lf} / f_c' < 0.08$. The different plots also report a bilinear fit with the corresponding coefficient of determination, R^2. It is observed that, for $f_{lf} / f_c' \geq 0.08$, $\left(P_{\max} - P_{f0}\right) / P_{f0}$ is described very well by the bilinear fit (R^2 = 0.982), whereas $\left(\overline{P}_{\max} - \overline{P}_{f0}\right) / \overline{P}_{f0}$ presents a higher dispersion (R^2 = 0.880). This result was expected, as c_f is directly related to the FRP confinement pressure achieved at the FRP failure, which is the predominant mechanism in determining the values of $P_{\max}$ and P_{f0}. This general behavior of higher dispersion for $\left(\overline{P}_{\max} - \overline{P}_{f0}\right) / \overline{P}_{f0}$ than for $\left(P_{\max} - P_{f0}\right) / P_{f0}$ is observed also for FRP-confined columns with $f_{lf} / f_c' < 0.08$; however, the dispersion is significantly higher than for the cases for which $f_{lf} / f_c' \geq 0.08$.

Similar to Figure 8, Figure 9(a) plots $\left(\overline{P}_{\max}-\overline{P}_{f0}\right)/\overline{P}_{f0}$ versus C_s for $f_{lf}/f_c' \geq 0.08$; Figure 9(b) plots $\left(\overline{P}_{\max}-\overline{P}_{f0}\right)/\overline{P}_{f0}$ versus C_s for $f_{lf}/f_c' < 0.08$; Figure 9(c) plots $\left(P_{\max}-P_{f0}\right)/P_{f0}$ versus C_s for $f_{lf}/f_c' \geq 0.08$; and Figure 9 (d) plots $\left(P_{\max}-P_{f0}\right)/P_{f0}$ versus C_s for $f_{lf}/f_c' < 0.08$. Also in this case, the different plots report a bilinear fit with the corresponding R^2. For $f_{lf}/f_c' \geq 0.08$, the bilinear fit is a good representation of both $\left(\overline{P}_{\max}-\overline{P}_{f0}\right)/\overline{P}_{f0}$ and $\left(P_{\max}-P_{f0}\right)/P_{f0}$ as functions of C_s. However, the dispersion is lower for $\left(\overline{P}_{\max}-\overline{P}_{f0}\right)/\overline{P}_{f0}$ ($R^2 = 0.957$) than for $\left(P_{\max}-P_{f0}\right)/P_{f0}$ ($R^2 = 0.921$), because C_s is directly related to the FRP confinement stiffness achieved when the axial strain in the concrete reaches $\varepsilon_{c,\max}$, which is the predominant mechanism in determining the values of $\overline{P}_{\max}$ and $\overline{P}_{f0}$. Also in this case, the dispersion observed for $f_{lf}/f_c' < 0.08$ is significantly higher than that for $f_{lf}/f_c' \geq 0.08$.

These results indicate that the effect of transverse steel confinement on the peak axial strength of FRP-confined RC columns is captured well by the two proposed coefficients c_f and C_s when $f_{lf}/f_c' \geq 0.08$. The use of coefficient c_f should be preferred when investigating the behavior of columns loaded up to their physical collapse (usually by fracture of the FRP confinement), whereas the coefficient C_s is better suited to describe the behavior of column designed to satisfy the deformation requirement imposed by Eq. (3). From the bilinear models in Figures 8 and 9, it is observed that $(P_{\max}-P_{f0})/P_{f0} = 0.05$ corresponds in average to a value of $c_f \approx 20\%$ for $f_{lf}/f_c' \geq 0.08$ and to $c_f \approx 28\%$ for $f_{lf}/f_c' < 0.08$; whereas $(\overline{P}_{\max}-\overline{P}_{f0})/\overline{P}_{f0} = 0.05$ corresponds to a value of $C_s \approx 15\%$ for $f_{lf}/f_c' \geq 0.08$ and to $C_s \approx 31\%$ for $f_{lf}/f_c' < 0.08$. Thus, it is recommended that the effect of simultaneous confinement by FRP and steel is considered whenever $c_f \geq 20\%$ and/or $C_s \geq 15\%$.It is also observed that, for typical values of $c_f \leq 100\%$ and

$C_s \leq 200\%$, the effect of transverse steel confinement can be very significant, with increases of the peak axial strength up to 30%-40% of the peak axial strength obtained by neglecting the transverse steel confinement effect. It is noted here that larger values of c_f and C_s than these typical values are still possible (as shown in Figure 8 and 9), albeit they are expected to be uncommon in practical applications, as they generally correspond to a combination of high transverse steel reinforcement and low FRP volumetric reinforcement ratios.

Conclusions

This paper investigates the effects of internal transverse steel confinement on the axial load-carrying capacity of FRP-confined reinforced concrete (RC) columns through a numerical parametric study. This parametric study is based on 1,152 nonlinear finite element (FE) analyses of FRP-confined RC columns considering a wide but realistic range of key parameters (i.e., type of FRP, volumetric FRP ratio, volumetric transverse steel ratio, concrete compressive strength, and column diameter). The nonlinear FE analyses are performed using a recently-developed confined concrete constitutive model able to accurately describe the simultaneous confinement effects of transverse steel reinforcement and FRP external wraps. The peak axial strengths of FRP-confined RC columns are estimated both considering the design limitation on maximum allowable concrete strain recommended by ACI 440.2R-17 (ACI 2017), $\overline{P}_{\max}$, and without imposing any strain limitation on the concrete, $P_{\max}$. For any given column, a reference unconfined column with strength P_0, and a reference FRP-only-confined column without transverse steel with strengths $\overline{P}_{f0}$ (with imposed strain design limitation) and P_{f0} (without imposed strain design limitation), are also considered. It is noteworthy that $\overline{P}_{\max}$ is a better representation of the columns' behavior for design purposes, whereas $P_{\max}$ provides a better estimate of the behavior of columns loaded up to physical collapse, as often done in experimental tests available in the literature.

It is observed that the normalized peak axial strength increment, $\left(\overline{P}_{\max} - P_0\right)/P_0$, of FRP-confined RC columns increases for increasing amounts of FRP and transverse steel, whereas it decreases for increasing unconfined concrete compressive strength. A small positive correlation is also found between $\left(\overline{P}_{\max} - P_0\right)/P_0$ and the ratio between concrete core and gross area, A_c / A_g. The FRP confinement alone can increase the column's peak axial strength by as much as approximately 90%. The interaction between FRP confinement and transverse steel confinement is highly nonlinear. In fact, the transverse steel confinement contribution to the peak axial strength of the columns increases with the amount of FRP for smaller FRP reinforcement ratios, and then decreases for increasing amounts of FRP for larger FRP reinforcement ratios. The threshold between smaller and larger FRP reinforcement ratios depends on the FRP material properties and the unconfined concrete compressive strength.

It is found that the design limitation on maximum allowable concrete strain recommended by ACI 440.2R-17 (ACI 2017) can have a significant impact (up to approximately 66% of the strength of the reference unconfined RC column) on the estimate of a column's peak axial strength, particularly for columns with high amounts of transverse steel and low amounts of FRP, and for columns with high amounts of FRP. For a given FRP confining stiffness, the effects of the strain design limitation are more pronounced for FRP materials with lower stiffness and higher ultimate strain, i.e., they are higher for GFRP than for CFRP confinement.

The contribution of the transverse steel confinement to the columns' peak axial strength can be very significant, with normalized peak axial strength increments $\left(\overline{P}_{\max} - \overline{P}_{f0}\right)/P_0$ as high as 111%. This relative contribution increases significantly with the transverse steel ratio and the A_c / A_g ratio, whereas it decreases for increasing FRP confining stiffness and unconfined concrete compressive strength. It is found that $\left(\bar{P}_{\max}-\bar{P}_{f0}\right)/P_0$ is almost independent of the FRP confining ratio f_{lf}/f_c' for $f_{lf}/f_c' \geq 0.08$.

In order to synthetically quantify the effects of the transverse steel confinement on the peak axial strength, two confinement pressure ratio coefficients are proposed in this study: $c_f=\left(f_{ls}\cdot A_c\right)/\left(f_{lf}\cdot A_g\right)$ and $C_s=\left(100 f_{ls}\cdot A_c\right)/\left(K_f\cdot A_g\right)$. It is found that, for $f_{lf}/f_c' \geq 0.08$, the relationships between $\left(\bar{P}_{\max}-\bar{P}_{f0}\right)/\bar{P}_{f0}$ and C_s, and between $\left(P_{\max}-P_{f0}\right)/P_{f0}$ and c_f are very well described by a bilinear fit. For typical values of $c_f \leq 100\%$ and $C_s \leq 200\%$, the transverse steel confinement effect can increase the peak axial strength up to 30%-40% of the peak axial strength estimated by neglecting this effect. It is concluded that, for values of $c_f \geq 20\%$ and $C_s \geq 15\%$, the effect of the transverse steel confinement should be considered in order to obtain accurate estimates of the peak axial strength of FRP-confined RC columns.

The synthetic parameters, c_f and C_s, identified in this study to describe the effects of transverse steel confinement in experimental and design applications, respectively, represent a preliminary but necessary step towards the development of improved predictive strength and design equations for FRP-confined RC columns subject to axial compression. Current research is ongoing to develop a design procedure for axially loaded FRP-confined RC columns based on rigorous structural reliability analysis procedures. Additional research is also needed to investigate and understand the effects of transverse steel confinement on the axial force-bending moment interaction behavior of FRP-confined RC columns.

Data Availability Statement

All data generated during the study appear in the submitted article. An executable version of the code used in the study is available from the corresponding author by request.

Acknowledgments

The authors gratefully acknowledge partial support of this research by the Brazilian National Council for Scientific and Technological Development (CNPq—Brazil). Any opinions, findings, conclusions, or recommendations expressed in this publication are those of the writers and do not necessarily reflect the views of the sponsors.

References

ACI (American Concrete Institute). 2017. *Guide for the design and construction of externally bonded FRP systems for strengthening concrete structures*. *ACI 440.2R-17*, Farmington Hills, MI: ACI.

Balan, T. A., Filippou, F. C., and Popov, E. P. 1997. "Constitutive model for 3D cyclic analysis of concrete structures." *J. Eng. Mech.*, 123(2), 143–153.

Bank, L. C. 2006. *Composites for Construction: Structural Design with FRP Materials*. John Wiley & Sons, Hoboken, NJ.

Cleveland, W. S. 1985. *The elements of graphing data*. *Wadsworth Publ. Co.*, Belmont, CA.

Demers, M., and Neale, K. W. 1999. "Confinement of reinforced concrete columns with fibre-reinforced composite sheets - an experimental study." *Can. J. Civ. Eng.*, 26(2), 226–241.

De Nicolo, B., Pani, L., and Pozzo, E. 1994. "Strain of concrete at peak compressive stress for a wide range of compressive strengths." *Mater. Struct.*, 27(4), 206–210.

Eid, R., Roy, N., and Paultre, P. 2009. "Normal- and high-strength concrete circular elements wrapped with frp composites." *J. Compos. Constr.*, 13(2), 113–124.

Fam, A. Z., and Rizkalla, S. H. 2001. "Confinement model for axially loaded concrete confined by circular fiber-reinforced polymer tubes." *ACI Struct. J.*, 98(4), 451–461.

Fardis, M. N., and Khalili, H. H. 1982. "FRP-encased concrete as a structural material." *Mag.*

Concr. Res., 34(121), 191–202.

Filippou, F. C., Popov, E. P., and Bertero, V. V. 1983. *Effects of bond deterioration on hysteretic behaviour of reinforced concrete joints*. *Earthq. Eng. Res. Cent.*, Report UCB/EERC-83/19, Univ. of California, Berkeley, CA.

Hu, D., and Barbato, M. 2014. "Simple and efficient finite element modeling of reinforced concrete columns confined with fiber-reinforced polymers." *Eng. Struct.*, 72, 113–122.

Hu, H., and Seracino, R. 2014. "Analytical model for FRP-and-steel-confined circular concrete columns in compression." *J. Compos. Constr.*, 18(3), A4013012.

Ilki, A., Peker, O., Karamuk, E., Demir, C., and Kumbasar, N. 2008. "FRP retrofit of low and medium strength circular and rectangular reinforced concrete columns." *J. Mater. Civ. Eng.*, 20(2), 169–188.

Karbhari, V. M., and Gao, Y. 1997. "Composite jacketed concrete under uniaxial compression - Verification of simple design equations." *J. Mater. Civ. Eng.*, 9(4), 185–193.

Lam, L., and Teng, J. G. 2003a. "Design-oriented stress-strain model for FRP-confined concrete." *Constr. Build. Mater.*, 17, 471–489.

Lam, L., and Teng, J. G. 2003b. "Design-oriented stress-strain model in rectangular columns." *J. Reinf. Plast. Compos.*, 22(13), 1149–1186.

Lee, J., Yi, C., Jeong, H., Kim, S. W., and Kim, J. K. 2010. "Compressive response of concrete confined with steel spirals and FRP composites." *J. Compos. Mater.*, 44(4), 481–504.

Li, Y. F., Lin, C. T., and Sung, Y. Y. 2003. "A constitutive model for concrete confined with carbon fiber reinforced plastics." *Mech. Mater.*, 35(3–6), 603–619.

Mander, J. 1983. "Seismic Design of Bridge Piers." Ph.D. Thesis, Univ. of Canterbury, Christchurch, New Zealand.

Mander, J., Priestley, M., and Park, R. 1988. "Theoretical stress-strain model for confined concrete." 114(8), 1804–1826.

Matthys, S., Toutanji, H., and Taerwe, L. 2006. "Stress-strain behavior of large-scale circular columns confined with FRP composites." *J. Struct. Eng.*, 132(1), 123–133.

Mazzoni, S., McKenna, F., Scott, M. H., and Fenves, G. L. 2006. *OpenSees Command Language Manual*. *Pacific Earthq. Eng. Res. Cent.*, Berkeley, CA.

Menegotto, M., and Pinto, P. E. 1973. "Method of analysis for cyclically loaded reinforced concrete plane frames including changes in geometry and nonelastic behavior of elements under combined normal force and bending." *IABSE Symp. Resist. Ultim. Deform. Struct. Acted by Well-Defined Repeated Loads*, International Association for Bridge and Structural Engineering, Zurich, Switzerland, 15–22.

Mirmiran, A., and Shahawy, M. 1996. "A new concrete-filled hollow FRP composite column." *Compos. Part B Eng.*, 27(3–4), 263–268.

Nanni, A., and Bradford, N. M. 1995. "FRP jacketed concrete under uniaxial compression." *Constr. Build. Mater.*, 9(2), 115–124.

Parvin, A., and Brighton, D. 2014. "FRP composites strengthening of concrete columns under various loading conditions." *Polymers*, 6, 1040–1056.

Piscesa, B., Attard, M. M., and Samani, A. K. 2018. "3D Finite element modeling of circular reinforced concrete columns confined with FRP using a plasticity based formulation." *Compos. Struct.*, 194, 478–493.

Popovics, S. 1973. "A numerical approach to the complete stress-strain curve of concrete." *Cem. Concr. Res.*, 3(5), 583–599.

Raza, S., Khan, M. K. I., Menegon, S. J., Tsang, H. H., and Wilson, J. L. 2019. "Strengthening and repair of reinforced concrete columns by jacketing: State-of-the-art review." *Sustain.*, 11(11), 3208.

Realfonzo, R., and Napoli, A. 2011. "Concrete confined by FRP systems: Confinement efficiency and design strength models." *Compos. Part B Eng.*, 42, 736–755.

Richart, F. E., Brandtzaeg, A., and Brown, R. L. 1929. "The failure of plain and spirally bound concrete in compression." *Bull. no. 190*, Univ. of Illinois, Eng. Experiment Station, Champaing, IL.

Rocca, S. 2007. "Experimental and analytical evaluation of FRP-confined large size reinforced concrete columns." Ph.D. Dissertation, Univ. of Missouri. Rolla, MO.

Rocca, S., Galati, N., and Nanni, A. 2006. *Evaluation of FRP strengthening of large-size reinforced concrete columns*. Report No. UTC-142. Univ. of Missouri-Rolla, MO.

Roy, N., Paultre, P., and Proulx, J. 2010. "Performance-based seismic retrofit of a bridge bent: Design and experimental validation." *Can. J. Civ. Eng.*, 37, 367–379.

Samaan, M., Mirmiran, A., and Shahawy, M. 1998. "Model of concrete confined by fiber composites." *J. Struct. Eng.*, 124(9), 1025–1031.

Shao, Y., Zhu, Z., and Mirmiran, A. 2006. "Cyclic modeling of FRP-confined concrete with improved ductility." *Cem. Concr. Compos.*, 28, 959–968.

Spoelstra, M. R., and Monti, G. 1999. "FRP-confined concrete model." *J. Compos. Constr.*, 3(3), 143–150.

Teng, J. G., Lin, G., and Yu, T. 2015. "Analysis-oriented stress-strain model for concrete under combined FRP-steel confinement." *J. Compos. Constr.*, 19(5), 04014084.

Toutanji, H. A. 1999. "Stress-strain characteristics of concrete columns externally confined with advanced fiber composite sheets." *ACI Mater. J.*, 96(3), 397–404.

Wang, Z., Wang, D., Smith, S. T., and Lu, D. 2012. "Experimental testing and analytical modeling of CFRP-confined large circular RC columns subjected to cyclic axial compression." *Eng. Struct.*, 40, 64–74.

Xiao, Y., and Wu, H. 2000. "Compressive behavior of concrete confined by carbon fiber composite jackets." *J. Mater. Civ. Eng.*, 12(2), 139–146.

Zignago, D., and Barbato, M. 2019. "Parametric study on the effect of steel confinement in short bridge piers retrofitted with externally-wrapped FRP." *MATEC Web Conf.*, 271, 01012.

Zignago, D., Barbato, M., and Hu, D. 2018. "Constitutive model of concrete simultaneously confined by FRP and steel for finite-element analysis of FRP-confined RC columns." *J. Compos. Constr.*, 22(6), 04018064.

Table 1 – Design parameters considered in the parametric study

Parameter	**Values**
Fiber type	Carbon (CFRP), Glass (GFRP)
CFRP ratio, ρ_f (%)	0, 0.25, 0.5, 1, 2, 3
GFRP ratio, ρ_f (%)	0, 0.5, 1, 2, 4, 6
Column diameter, D (mm)	150, 300, 600, 1200
Concrete strength, f_c' (MPa)	20, 30, 50, 70
Transverse steel ratio, ρ_{st} (%)	0, 0.5, 1, 2, 3, 4

Table 2 - Material properties used in the FE simulations

Material	**Properties**	**Value**
Transverse steel	Yield strength, f_{yt} (MPa)	450
	Young's modulus, E_{st} (GPa)	200
Longitudinal steel	Strain hardening ratio, b (-)	0.005
	Yield strength, f_{yl} (MPa)	450
	Young's modulus, E_{sl} (GPa)	200
	Longitudinal steel ratio, ρ_{sl} (%)	1.0
CFRP	Tensile strength, f_{fu} (MPa)	1200
	Young's modulus, E_f (GPa)	100
GFRP	Tensile strength, f_{fu} (MPa)	600
	Young's modulus, E_f (GPa)	25

Figure 1 – Box-and-whisker plots of $\left(\overline{P}_{\max}-P_0\right)/P_0$ for: (a) FRP confining stiffness; (b) diameter; (c) concrete strength; and (d) transverse steel ratio

Figure 2 – Effect of FRP confinement ratio on $\left(\overline{P}_{\max}-P_0\right)/P_0$

Figure 3 – Transverse steel confinement effect on $\left(\overline{P}_{\max}-P_0\right)/P_0$ for FRP-confined columns with: (a) f_c' = 30 MPa for varying amount of CFRP and column diameter, and (b) D = 600 mm and K_f = 0.5 GPa for varying FRP type and concrete strength

Figure 4 – Stress-strain responses of confined concrete with f_c' = 30 MPa for different FRP and transverse steel confinement configurations

Figure 5 – Effect of concrete strain design limitation provision on columns' peak axial strength: (a) for varying amount of FRP and column diameter, and (b) for varying FRP material and concrete compressive strength

Figure 6 – Box-and-whisker plots of $\left(\overline{P}_{\max}-\overline{P}_{f0}\right)/P_0$ for: (a) FRP confining stiffness; (b) diameter; (c) concrete strength; and (d) transverse steel ratio

Figure 7 - Effect of FRP confinement ratio on relative peak axial strength increment with respect to the reference FRP-only-confined columns

Figure 8 - Steel confinement contribution to normalized peak axial strength increment versus relative confinement effect coefficient c_f

Figure 9 - Steel confinement contribution to normalized peak axial strength increment versus relative confinement effect coefficient C_s

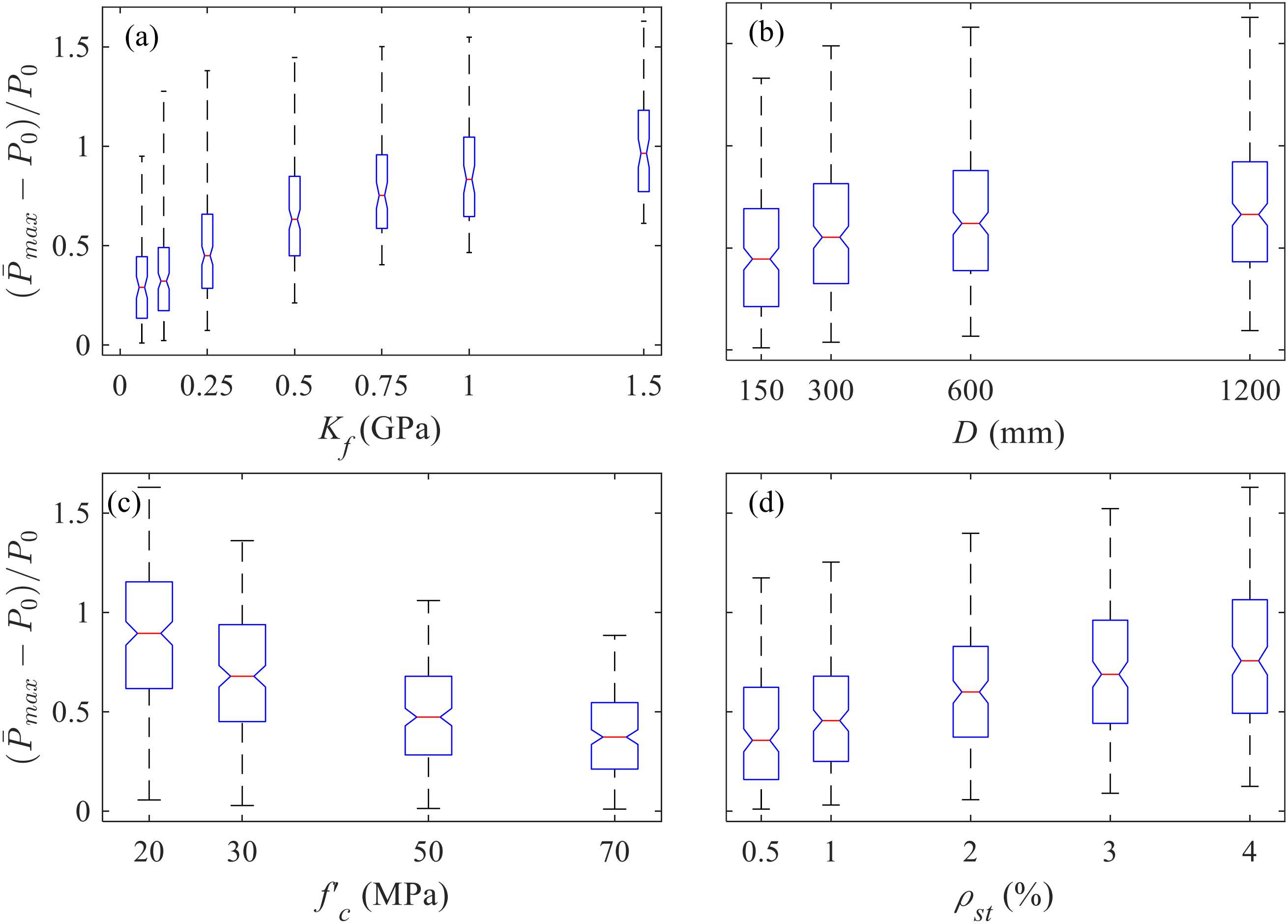
(a)
(b)
(c)
(d)
$(\bar{P}_{max} - P_0)/P_0$
$(\bar{P}_{max} - P_0)/P_0$
0
0.5
1
1.5
0
0.5
1
1.5
0
0.25
0.5
0.75
1
1.5
K_f (GPa)
150
300
600
1200
D (mm)
20
30
50
70
f'_c (MPa)
0.5
1
2
3
4
ρ_{st} (%)

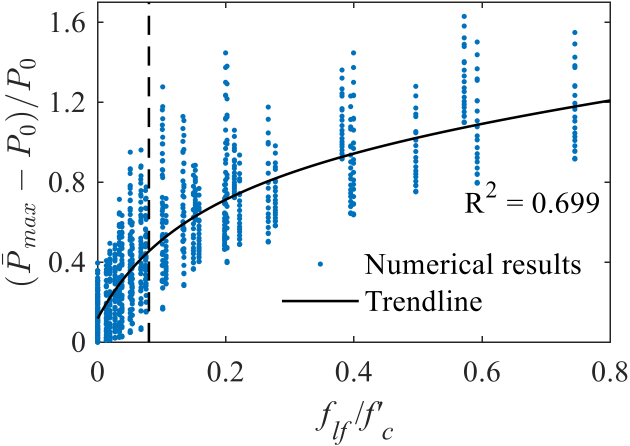
$(\bar{P}_{max} - P_0)/P_0$
1.6
1.2
0.8
0.4
0
0
0.2
0.4
0.6
0.8
f_{lf}/f'_c
$R^2 = 0.699$
Numerical results
Trendline

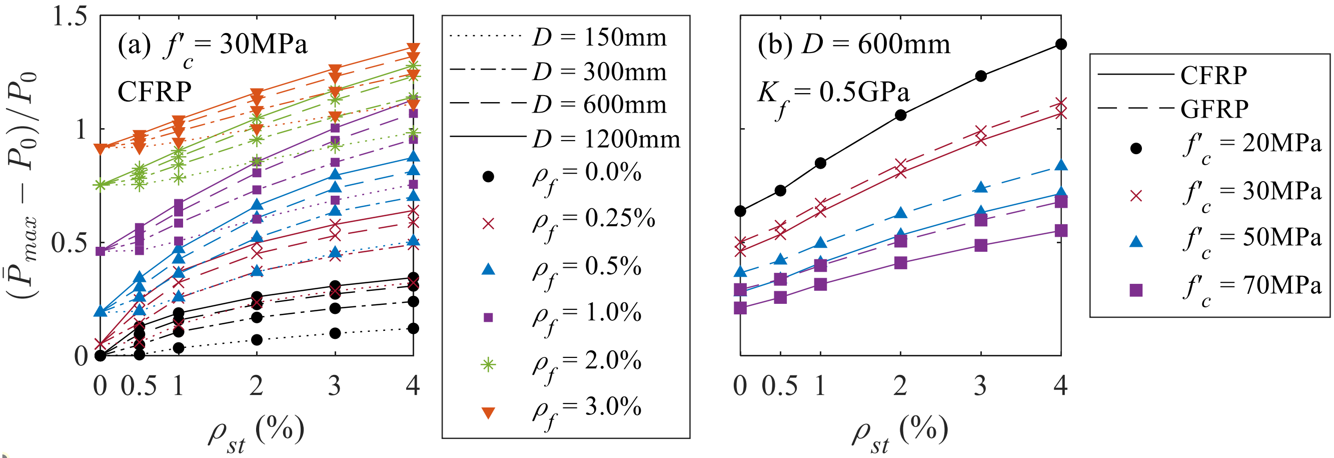
(a) $f'_c = 30\text{MPa}$
CFRP
$(\bar{P}_{max} - P_0)/P_0$
0
0.5
1
1.5
0
0.5
1
2
3
4
ρ_{st} (%)
$D = 150\text{mm}$
$D = 300\text{mm}$
$D = 600\text{mm}$
$D = 1200\text{mm}$
● $\rho_f = 0.0\%$
× $\rho_f = 0.25\%$
▲ $\rho_f = 0.5\%$
■ $\rho_f = 1.0\%$
✳ $\rho_f = 2.0\%$
▼ $\rho_f = 3.0\%$
(b) $D = 600\text{mm}$
$K_f = 0.5\text{GPa}$
0
0.5
1
2
3
4
ρ_{st} (%)
CFRP
GFRP
● $f'_c = 20\text{MPa}$
× $f'_c = 30\text{MPa}$
▲ $f'_c = 50\text{MPa}$
■ $f'_c = 70\text{MPa}$

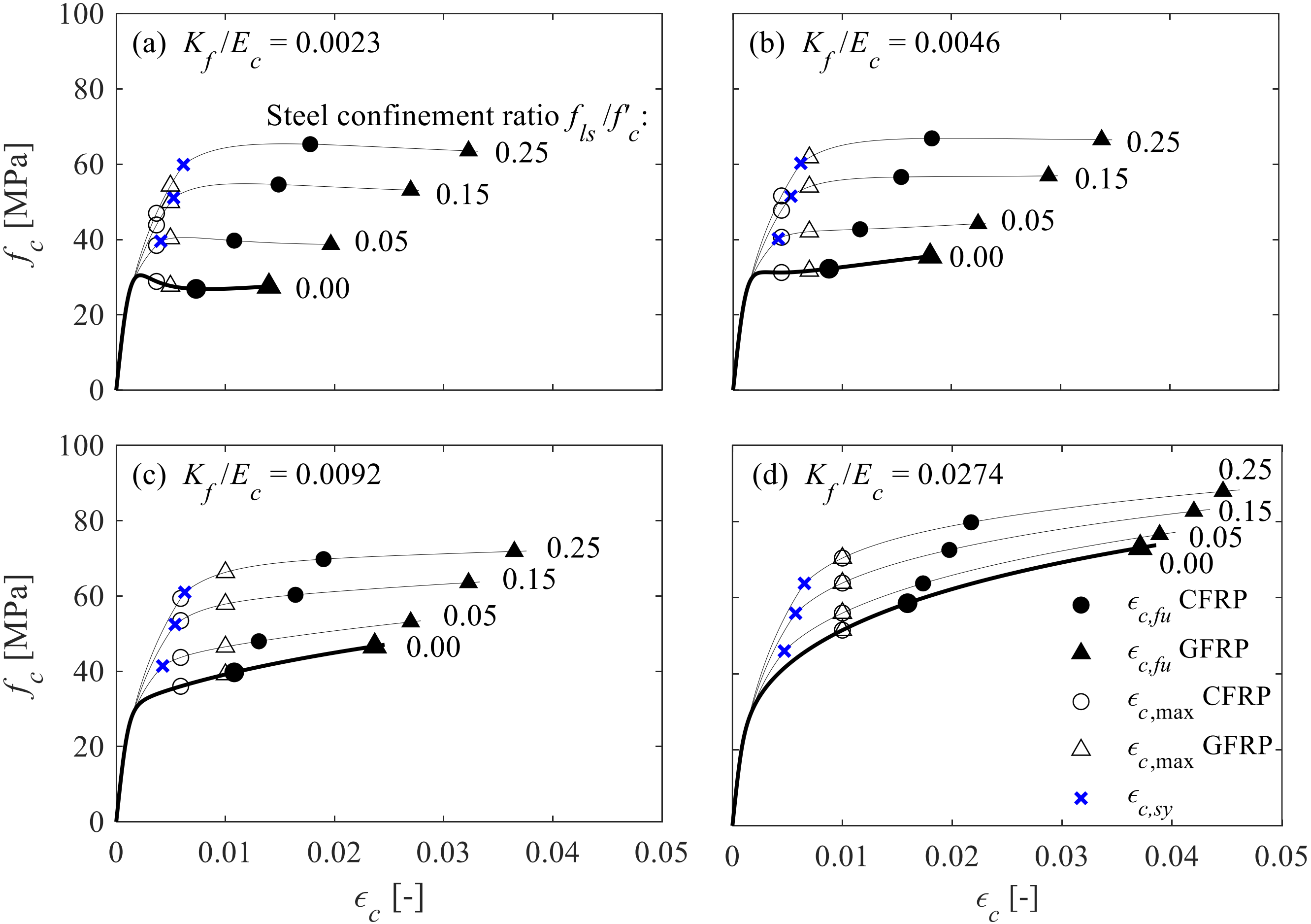
(a) K_f/E_c = 0.0023
(b) K_f/E_c = 0.0046
(c) K_f/E_c = 0.0092
(d) K_f/E_c = 0.0274
Steel confinement ratio f_{ls}/f'_c:
0.25
0.15
0.05
0.00
f_c [MPa]
ϵ_c [-]
0
20
40
60
80
100
0
0.01
0.02
0.03
0.04
0.05
● $\epsilon_{c,fu}$ CFRP
▲ $\epsilon_{c,fu}$ GFRP
○ $\epsilon_{c,\max}$ CFRP
△ $\epsilon_{c,\max}$ GFRP
× $\epsilon_{c,sy}$

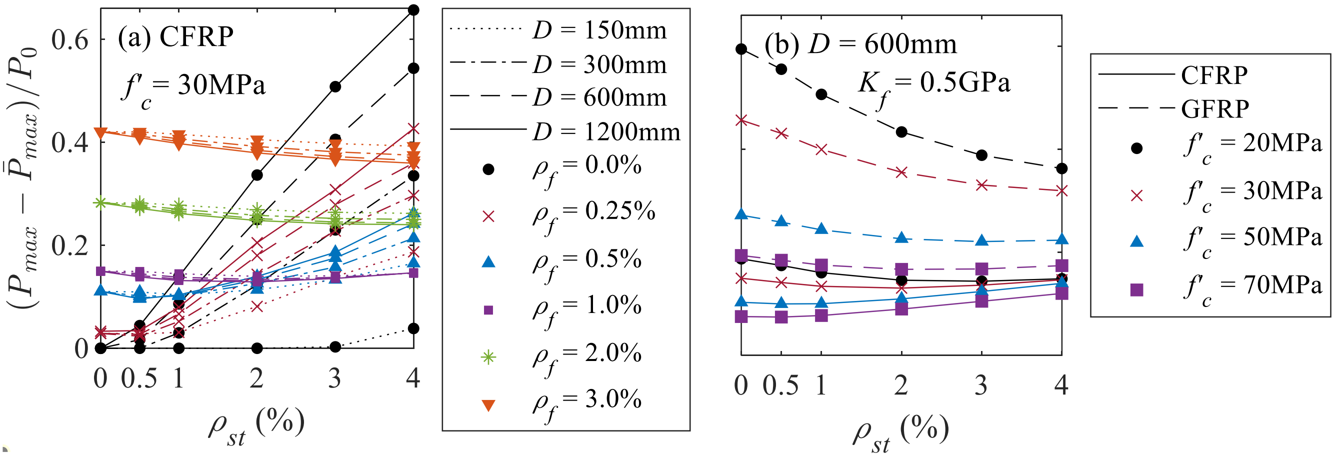
(a) CFRP
$f'_c = 30$MPa
$(P_{max} - \bar{P}_{max})/P_0$
0
0.2
0.4
0.6
0
0.5
1
2
3
4
ρ_{st} (%)
$D = 150$mm
$D = 300$mm
$D = 600$mm
$D = 1200$mm
$\rho_f = 0.0\%$
$\rho_f = 0.25\%$
$\rho_f = 0.5\%$
$\rho_f = 1.0\%$
$\rho_f = 2.0\%$
$\rho_f = 3.0\%$
(b) $D = 600$mm
$K_f = 0.5$GPa
0
0.5
1
2
3
4
ρ_{st} (%)
CFRP
GFRP
$f'_c = 20$MPa
$f'_c = 30$MPa
$f'_c = 50$MPa
$f'_c = 70$MPa

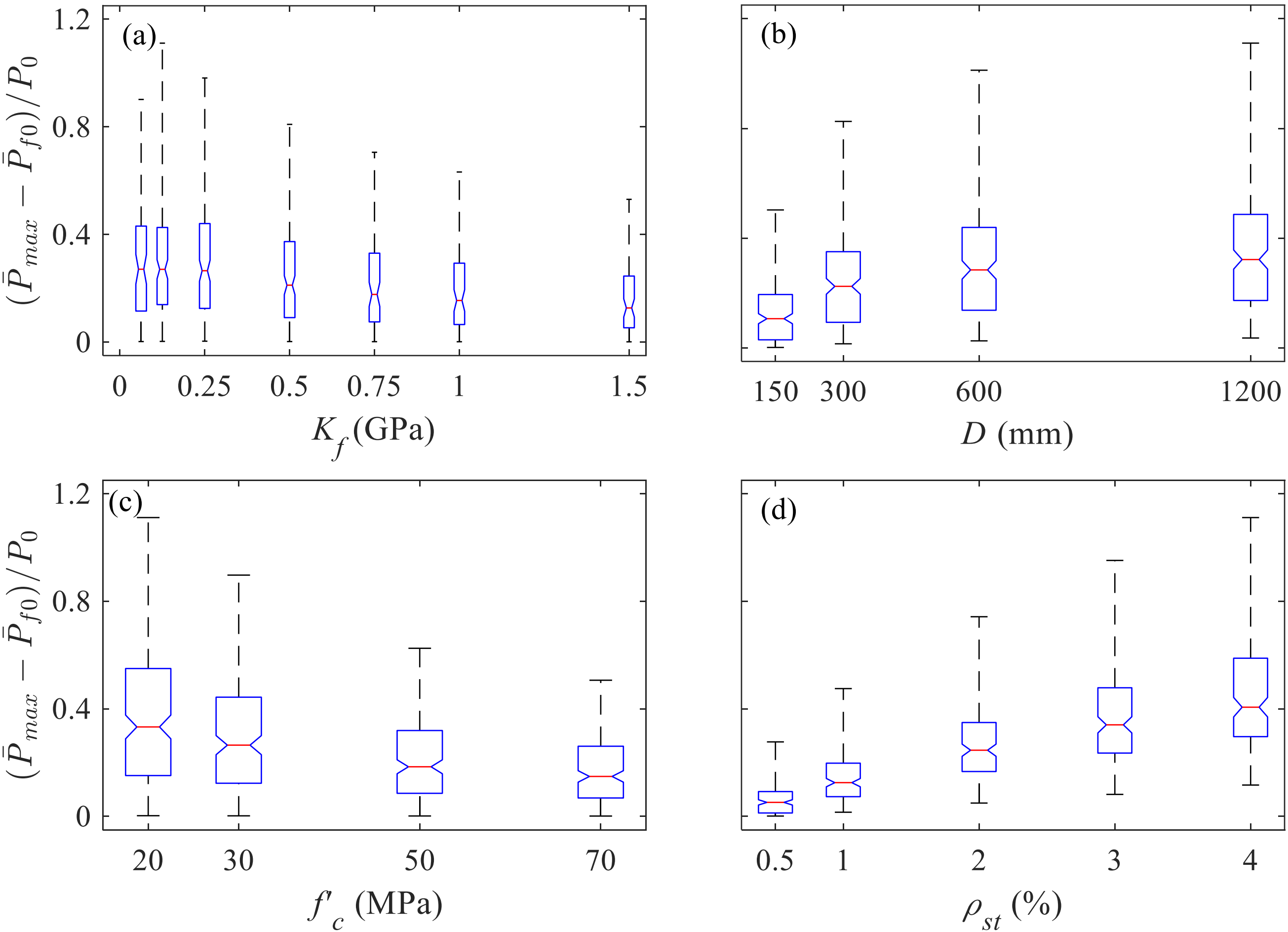
(a)
(b)
(c)
(d)
$(\bar{P}_{max} - \bar{P}_{f0})/P_0$
1.2
0.8
0.4
0
0
0.25
0.5
0.75
1
1.5
K_f (GPa)
150
300
600
1200
D (mm)
20
30
50
70
f'_c (MPa)
0.5
1
2
3
4
ρ_{st} (%)

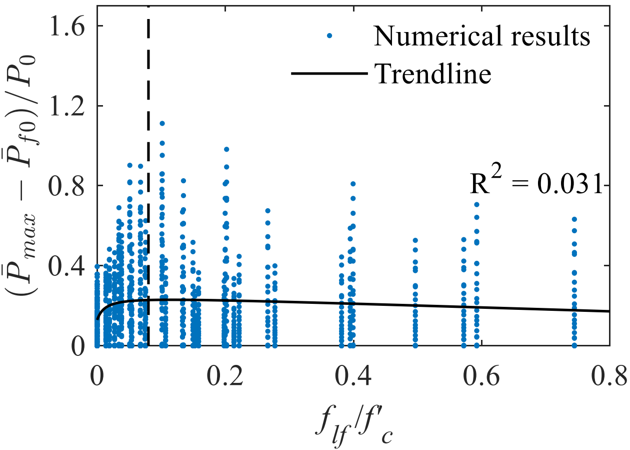

Numerical results
Trendline
$R^2 = 0.031$
$(\bar{P}_{max} - \bar{P}_{f0})/P_0$
1.6
1.2
0.8
0.4
0
0
0.2
0.4
0.6
0.8
f_{lf}/f'_c

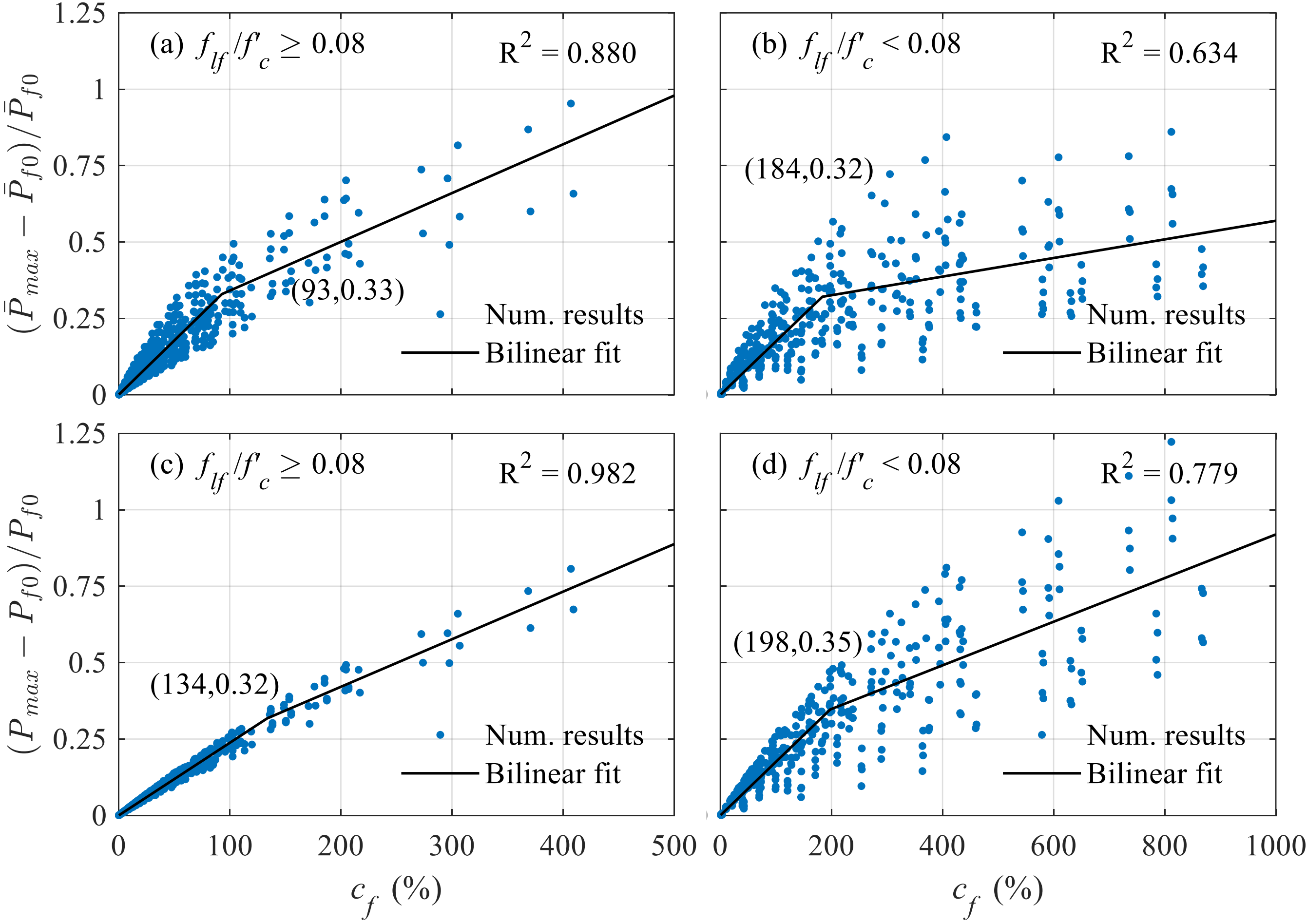
(a) $f_{lf}/f'_c \geq 0.08$
$R^2 = 0.880$
(93,0.33)
(b) $f_{lf}/f'_c < 0.08$
$R^2 = 0.634$
(184,0.32)
(c) $f_{lf}/f'_c \geq 0.08$
$R^2 = 0.982$
(134,0.32)
(d) $f_{lf}/f'_c < 0.08$
$R^2 = 0.779$
(198,0.35)
Num. results
Bilinear fit
$(\bar{P}_{max} - \bar{P}_{f0})/\bar{P}_{f0}$
$(P_{max} - P_{f0})/P_{f0}$
c_f (%)
0
0.25
0.5
0.75
1
1.25
100
200
300
400
500
600
800
1000

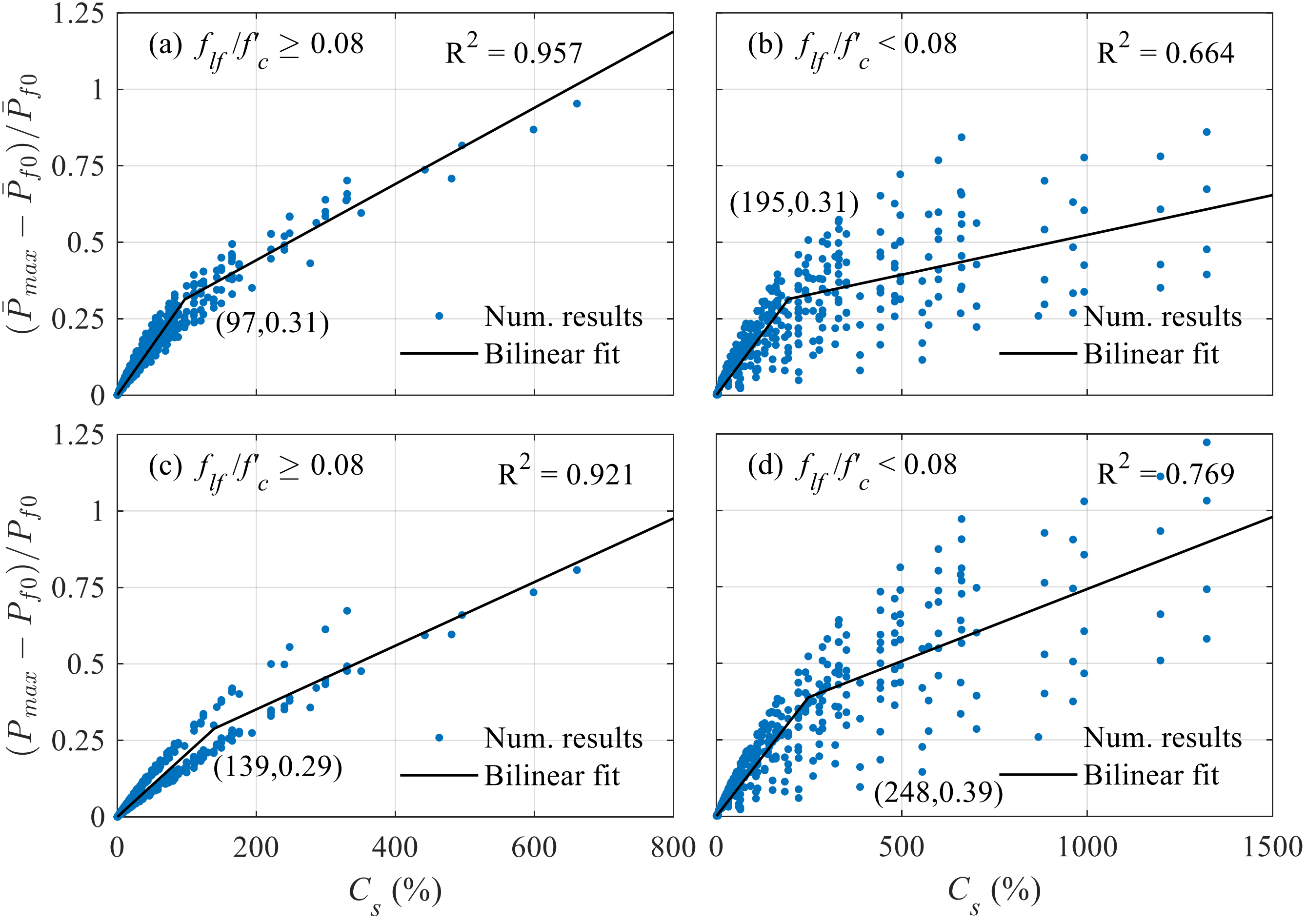
(a) $f_{lf}/f'_c \geq 0.08$
$R^2 = 0.957$
(97,0.31)
(b) $f_{lf}/f'_c < 0.08$
$R^2 = 0.664$
(195,0.31)
(c) $f_{lf}/f'_c \geq 0.08$
$R^2 = 0.921$
(139,0.29)
(d) $f_{lf}/f'_c < 0.08$
$R^2 = 0.769$
(248,0.39)
Num. results
Bilinear fit
$(\bar{P}_{max} - \bar{P}_{f0})/\bar{P}_{f0}$
$(P_{max} - P_{f0})/P_{f0}$
0
0.25
0.5
0.75
1
1.25
0
200
400
600
800
0
500
1000
1500
C_s (%)